Redox Biology 34 (2020) 101459

Contents lists available at ScienceDirect

Redox Biology

journal homepage: www.elsevier.com/locate/redox

CircRNA_0001449 disturbs phosphatidylinositol homeostasis and AKT activity by enhancing *Osbpl5* translation in transient cerebral ischemia

Fei-Fei Shang[a], Li Luo[a], Jianghong Yan[a], Qiubo Yu[a], Yongzheng Guo[b], Yuchen Wen[a], Xiao-Li Min[c], Ling Jiang[d], Xiang He[d,e,*], Wei Liu[f,**]

[a] Institute of Life Science, Chongqing Medical University, Chongqing, 400016, China
[b] Division of Cardiology, The First Affiliated Hospital of Chongqing Medical University, Chongqing, 400016, China
[c] Department of Cerebrovascular Diseases, The Second Affiliated Hospital of Kunming Medical University, Kunming, Yunnan Province, 650101, China
[d] Department of Anesthesiology, Guizhou Provincial People's Hospital, Guiyang, Guizhou Province, 550002, China
[e] Department of Neuroscience, Yale School of Medicine, New Haven, CT, 06510, USA
[f] Department of Anesthesiology, Huashan Hospital, Fudan University, Shanghai, 200040, China

ARTICLE INFO

Keywords:
Cerebral ischemia
Lipids and lipoprotein metabolism
Non-coding RNA
AKT

ABSTRACT

Phosphatidylinositol-3,4,5-trisphosphate [PI(3,4,5)P3] is a phosphorylated derivative of phosphatidylinositol 4-phosphate [PI(4)P] and phosphatidylinositol 4,5-bisphosphate [PI(4,5)P2], which recruit and activate AKT in the plasma membrane (PM) to promote cellular survival. ORP5 anchors at the endoplasmic reticulum (ER)-PM contact sites and acts as a PI(4)P and PI(4,5)P2/phosphatidylserine (PS) exchanger. Here, a lipidomics analysis of the sensorimotor cortex revealed that transient middle cerebral artery occlusion (tMCAO) disturbs the homeostasis of phosphatidylinositols (PIs) and PS between the PM and ER. Conditional knockout mice showed that ORP5 contributes to this abnormal distribution. Abolishing the ORP5 gene significantly inhibited apoptosis and autophagy. RNA sequencing and RNA pull down analyses confirmed a competing endogenous RNA pathway in which circ_0001449 sponges miR-124-3p and miR-32-5p to promote *Osbpl5* translation. Our data showed that circRNA_0001449 regulates membrane homeostasis via ORP5 and is involved in the AKT survival pathway.

1. Introduction

Transient occlusion of a cerebral artery leads to delayed cell death that occurs after reperfusion, and abundant accumulation of damaged membranous organelles, including the endoplasmic reticulum (ER), plasma membrane (PM), late endosomes, occurs over time in cells destined to undergo cell death [1,2]. Among these damaged membranous organelles, the ER is essential for cellular survival, and ER stress-induced apoptosis and autophagy are implicated in the pathophysiology of several cerebral diseases [3–5]. In addition, the PM is a control centre for autophagosomes and apoptotic body formation [6–8]. Therefore, homeostasis of the PM and ER may determine cell fate after cerebral ischemic injury.

Cellular compartmentalization into membranous organelles requires precise spatiotemporal distribution of certain lipids that serve as organelle identity signatures [9]. The intracellular trafficking of lipids is, therefore, central to membrane homeostasis. The movement of specific lipids among organelles involves vesicular trafficking or lipid transfer proteins (LTPs). Notably, the main site for cellular lipid synthesis is the ER [10]. Membrane tubules of the ER dynamically spread to form close membrane contact sites with other organelles. The gaps of these contact sites are highly enriched LTPs [11]. One class of proteins mediating these contacts is oxysterol-binding proteins (OSBPs) and OSBP-related proteins (ORPs), which are believed to function selectively as different sterol sensors or transporters [10]. Recent reports have focused on ORP5 and ORP8, which tether the ER to the PM via the interaction of their pleckstrin homology (PH) domains with phosphatidylinositol 4-phosphate [PI(4)P] and phosphatidylinositol 4,5-bisphosphate [PI(4,5)P2] in these membranes. OSBP-related domains mediate PI(4)P or PI(4,5)P2 exchange with phosphatidylserine (PS) between the bilayers [12,13].

In eukaryotic cells, phosphatidylinositol (PI) and its phosphorylated derivatives represent quantitatively minor components of cell membranes. Despite their low levels, inositol phospholipids play critical roles in the control of signal transduction and cell survival [14]. The proper balance of the PIs levels are maintained not only through the

* Corresponding author. Department of Anesthesiology, Guizhou Provincial People's Hospital, Guiyang, 550002, China.
** Corresponding author.
E-mail addresses: hexgmc@163.com (X. He), liuwei605@163.com (W. Liu).

https://doi.org/10.1016/j.redox.2020.101459
Received 26 December 2019; Received in revised form 2 February 2020; Accepted 7 February 2020
Available online 10 February 2020

Nonstandard abbreviations and acronyms

ER	Endoplasmic reticulum
PM	Plasma membrane
OSBP	Oxysterol-binding protein
ORP	OSBP-related protein
PI(4)P	Phosphatidylinositol 4-phosphate
PI(4,5)P2	Phosphatidylinositol 4,5-bisphosphate
PI(3,4,5)P3	Phosphatidylinositol-3,4,5-trisphosphate
PS	Phosphatidylserine
PI	Phosphatidylinositol
circRNA	Circular RNA
tMCAO	Transient middle cerebral artery occlusion

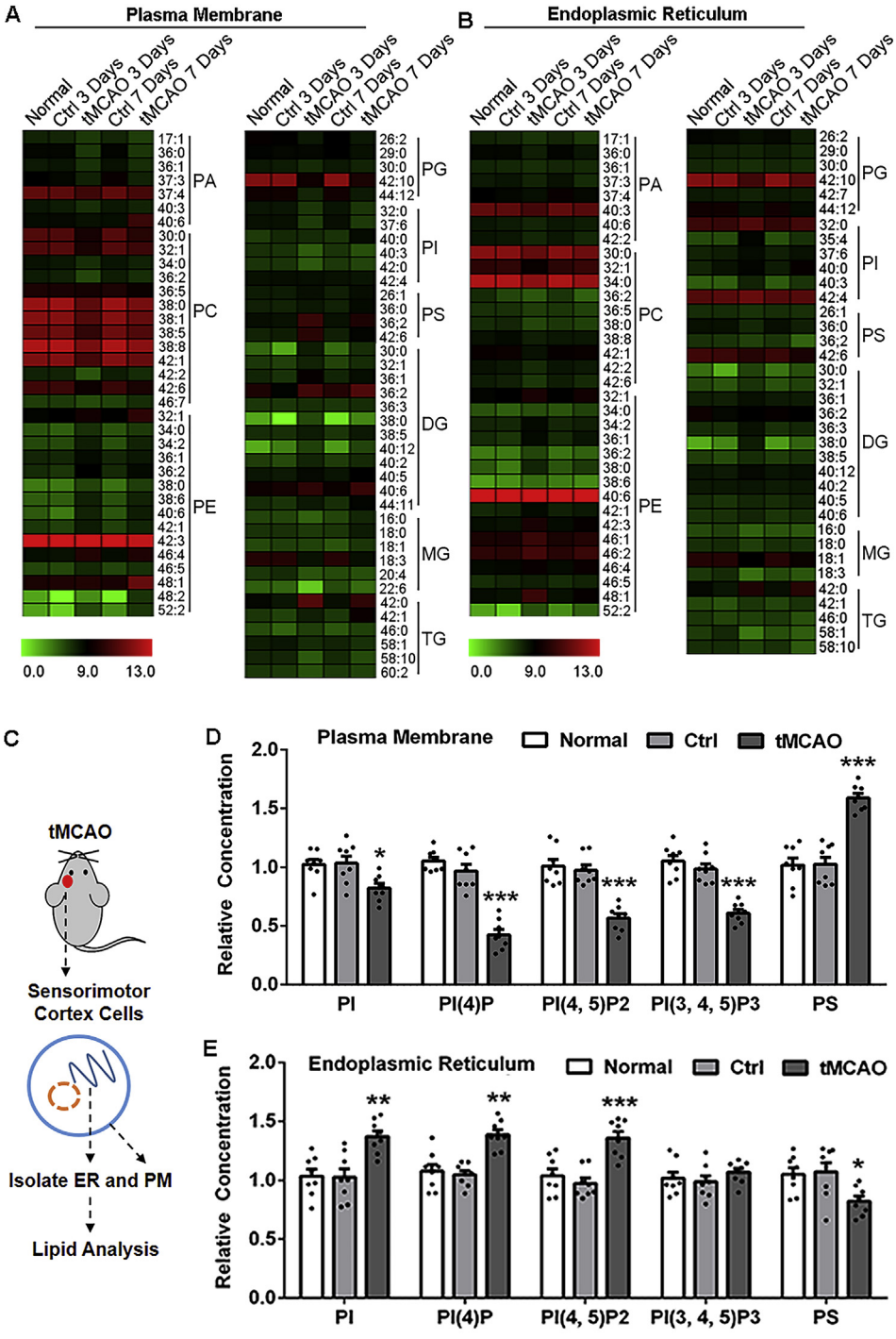

Fig. 1. Lipid homeostasis of the sensorimotor cortex is disrupted in transient middle cerebral artery occlusion (tMCAO) mice. (A, B) After 1 h of occlusion, lipid metabolomics detected lipid alterations between the endoplasmic reticulum (ER) and plasma membrane (PM); n = 5–13 per group. **(C)** Illustration of the experimental process. **(D, E)** Phosphatidylinositol (PI) and phosphorylated PIs show opposite changes from those of phosphatidylserine (PS), as shown by ELISA; n = 8 per group. *, compared with the Ctrl group.

regulation of PI kinases and phosphatases but also through transfer proteins, such as ORP5 and ORP8[15]. PI(4,5)P2 is produced from PM PI (4)P by PIP 5-kinase (PIP5K), and PI(4)P is generated from PI by PI4-kinase (PI4K). PI, PI(4)P and PI(4,5)P2 are important PIs found in the PM and serve as precursors for a phosphatidylinositol 3-kinase (PI3K)-generated messenger, phosphatidylinositol-3,4,5-trisphosphate [PI (3,4,5)P3][16]. Furthermore, AKT and PDK1, which contain the PH domain, are recruited to the PM by PI(3,4,5)P3. This colocalization allows PDK1 to phosphorylate AKT at T308. AKT is also phosphorylated at a hydrophobic motif, S473, by mTORC2. Activated AKT plays a critical role in cell survival, growth, and differentiation [17]. Thus, PI, PI(4)P, and PI(4,5)P2 are critical for the maintenance of PI(3,4,5)P3 in the PM to protect the cells from ischemia-reperfusion injury.

Circular RNAs (circRNAs) have recently been described as novel regulatory non-coding RNAs. These molecules are typically generated through a process of backsplicing from exons, and introns form a covalent bond linking the 3′ and 5′ ends [18]. Some circRNAs play a potential role as competitive endogenous RNAs to compete for miRNA-binding sites, thus affecting miRNA activities. They can inhibit the levels of target miRNAs by absorbing miRNAs and, thus, can liberate the mRNA transcripts targeted by the miRNAs [19]. Studies have shown that circRNAs play important roles in stroke. For example, circRNA

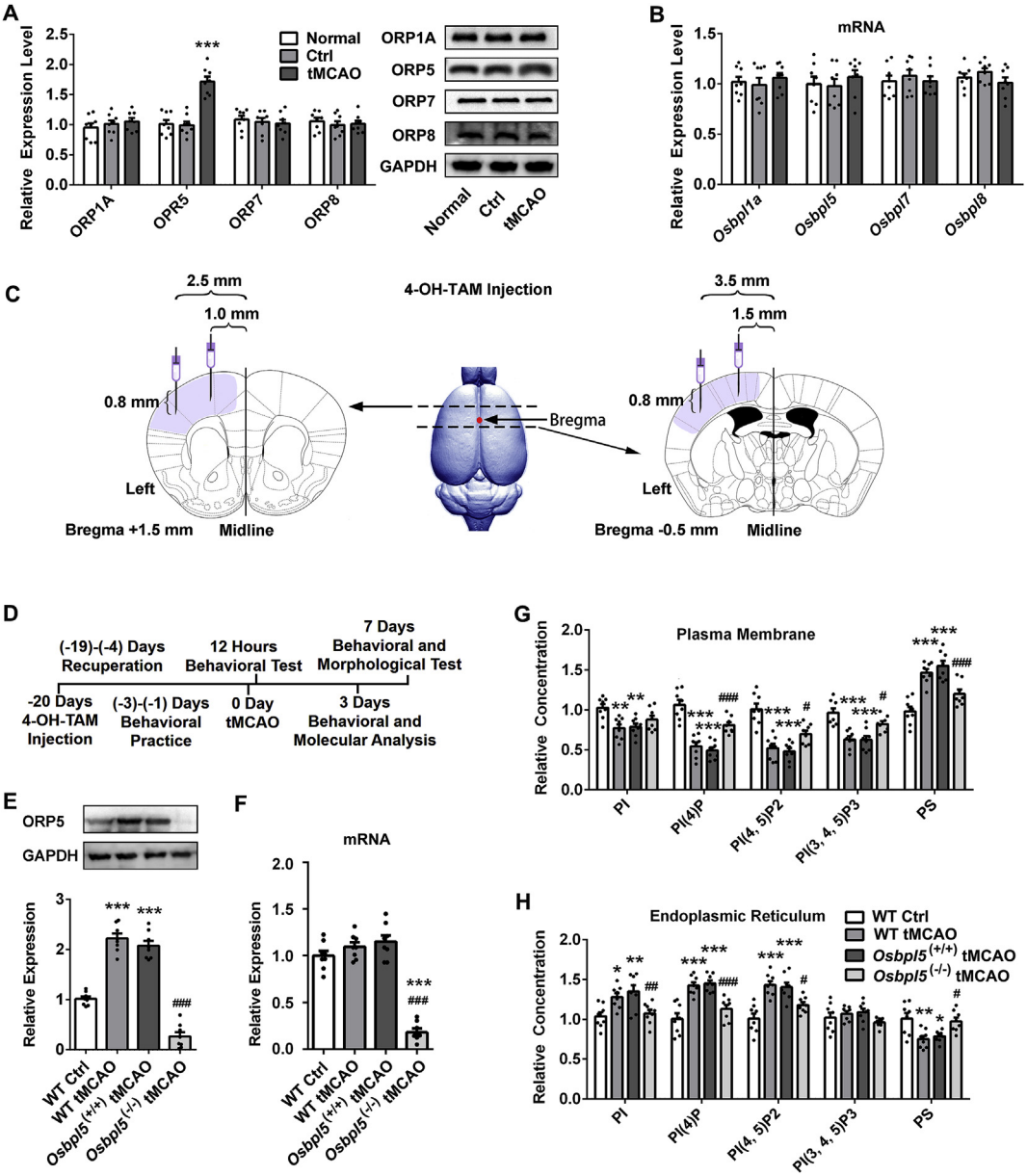

Fig. 2. After ischemia injury, ORP5 contributes to the disruption of PI, phosphorylated PIs and PS. **(A)** Immunoblotting shows that the ORP5 protein is specifically upregulated in the sensorimotor cortex; n = 8 per group. **(B)** The transcript levels of several ORP genes, including *Osbpl5*, were not significantly changed after transient ischemia; n = 8 per group. **(C)** Cartoon representation of the *Osbpl5* conditional knockout mice were injected with 4-hydroxy-tamoxifen (4-OH-TAM) in the sensorimotor cortex. The coordinate of the bregma is (0, 0). **(D)** Illustration of the experimental procedure using *Osbpl5* knockout or wild-type (WT) mice. **(E)** The ORP5 protein was abolished in the ischemic sensorimotor cortex of *Osbpl5* $^{(-/-)}$ mice, even though ischemia induced ORP5 upregulation; n = 8 per group. *Osbpl5* $^{(+/+)}$ is a heterozygous *Cre* strain that does not have insertions of the *loxP* site flanked sequence in the *Osbpl5* gene. *Osbpl5* $^{(-/-)}$ contains a *loxP* site where exons 8 and 9 of *Osbpl5* were knocked out by heterozygous *Cre* expression. Both *Osbpl5* $^{(+/+)}$ and *Osbpl5* $^{(-/-)}$ mice were injected with 4-OH-TAM to induce *Cre* expression. **(F)** The *Osbpl5* mRNA in WT tMCAO mice remained unchanged. The knockout effect was also successfully evaluated in *Osbpl5* $^{(-/-)}$ tMCAO mice by RT-PCR; n = 8 per group. **(G, H)** In the PM and ER, the transient ischemia-altered PIs and PS concentrations were recovered by *Osbpl5* knockout; n = 8 per group. *, compared with the Ctrl or WT Ctrl group; #, compared with the *Osbpl5* $^{(+/+)}$ tMCAO group.

Hectd1 acts as a competitive endogenous RNA to sponge miR-142 and contributes to ischemic stroke via astrocyte activation [20]. CircRNA TLK1 aggravates ischemic injury via miR-335-3p/TIPARP [21]. However, whether circRNAs could regulate the survival molecule AKT is unknown.

Here, lipidomics analysis and conditional knockout mice clearly demonstrated that ORP5 disrupted the PIs/PS homeostasis in the PM and ER after transient middle cerebral artery occlusion (tMCAO) injury. PI(3,4,5)P3 deficiency in the PM induced by increased ORP5 protein levels inhibited the survival effect of AKT. In addition, the mRNA level of *Osbpl5* was unaltered in the injured sensorimotor cortex. RNA sequencing coupled with RNA pull down and luciferase reporter assays demonstrated that miR-124-3p and miR-32-5p could inhibit the translation of *Osbpl5* mRNA under physiological conditions. Notably, we found that miR-124-3p, but not miR-32-5p, was dramatically enriched in tMCAO mice. Using RNA sequencing, we further found that circ_0001449 competes with *Osbpl5* mRNA to bind to miR-124-3p and miR-32-5p in ischemic mice. This process releases miR-124-3p and miR-32-5p from *Osbpl5* mRNA, which enhances the ORP5 protein level, thus reducing AKT activity. Finally, our results confirmed the critical importance of ORP5 in cerebral ischemia and showed, for the first time, that hsa_circ_0001449 regulates AKT phosphorylation via ORP5 translational control.

2. Methods

Detailed methods section is available in the Supplementary Materials.

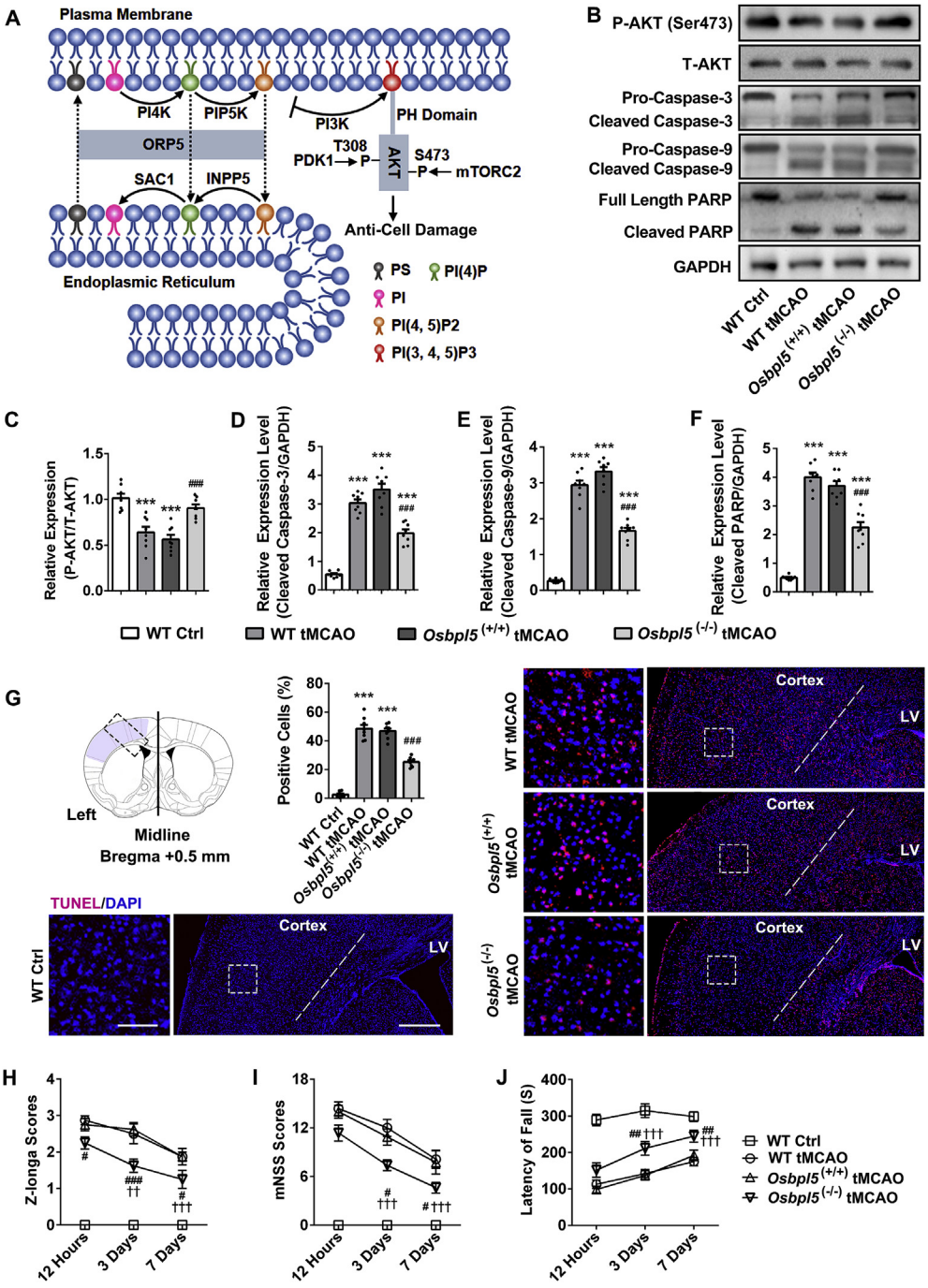

Fig. 3. ORP5 decreases PI(3,4,5)P3 in PM to weaken the AKT-mediated cell protective effect. **(A)** The schematic shows the possible ORP5 function, which is based on the previous results and literature. Ischemia injury elevates ORP5 to decrease PI(4)P and PI(4,5)P2 in the PM. This change reduces the PI(3,4,5)P3 supply, which decreases the AKT anchor to PI(3,4,5)P3. Finally, AKT phosphorylation and activation are impaired, weakening the protective effects against cell damage. In the ER, enriched PI(4)P and PI(4,5)P2 are dephosphorylated by SAC1 and INPP5 to form PI. **(B)** Representative blotting bands of AKT and apoptosis markers. **(C–F)** Statistical analysis of the blot bands. The results show that phosphorylated AKT (P-AKT) is increased and cleaved caspase-3, caspase-9, and PARP are decreased in the sensorimotor cortex of *Osbpl5* $^{(-/-)}$ tMCAO mice; n = 8 per group. **(G)** Confocal microscopy images showing apoptosis-positive cells in *Osbpl5* knockout mice by TUNEL assays. The dotted box in the schematic indicates the area of 4-OH-TAM injection that was captured by microscopy; n = 8 per group. Bars = 100 μm and 500 μm. **(H–J)** The enhanced neurobehavioural manifestations in *Osbpl5* $^{(-/-)}$ tMCAO mice were indicated by Z-longa, mNSS, and rotarod tests; n = 8 per group. *, compared with the WT Ctrl group; #, compared with the *Osbpl5* $^{(+/+)}$ tMCAO group; †, compared with the 12 h reperfusion in *Osbpl5* $^{(-/-)}$ tMCAO group.

3. Results

3.1. Transient ischemia disturbed the lipid homeostasis of the PM and ER

We first analysed the lipid composition of the isolated PM and ER prepared from normal, control and injured sensorimotor cortices using liquid chromatography-tandem mass spectrometry (Fig. 1C). Supervised orthogonal partial least-squares discriminant analysis was then performed to explore the metabolic differences at 3 days and 7 days after reperfusion. Compared with those of the normal or control group, the score plots of the 3-day and 7-day groups visually showed a clear differentiation in both positive (Supplementary Fig. 1A) and negative ion mode (Supplementary Fig. 1B). To confirm the quality and effectiveness of the orthogonal partial least-squares discriminant analysis model, we applied a permutation method. The R^2 and Q [2] values close to 1 indicated that the model had good fitness and predictive abilities (Supplementary Figs. 1A and 1B).

Next, the significantly differentially abundant lipids, which had fold changes > 2, variable importance plots > 1 and $p < 0.05$ from one-way ANOVA, are summarized in the heat map (Fig. 1A and 1B). In total, we identified 74 specific lipids that differed in abundance in the PM and 70 lipids in the ER. Among these lipids, 65 lipids were detected in both biological membranes.

3.2. Transient ischemia caused an abnormal distribution of PIs and PS between the PM and ER

We noticed lipidomics data that PI was significantly decreased in the PM but profoundly enhanced in the ER at both 3 and 7 days. Moreover, the PS level was slightly upregulated in the PM but clearly downregulated in the ER. We further verified these results by ELISAs on day 3. In the PM, the results showed that the PI and its derivatives, PI(4)P, PI(4,5)P2, and PI(3,4,5)P3, were significantly decreased in the tMCAO mice compared with those in the control mice [Fig. 1D, PI: $F_{(2, 21)} = 5.92$; PI(4)P: $F_{(2, 21)} = 55.33$; PI(4,5)P2: $F_{(2, 21)} = 27.67$; PI(3,4,5)P3: $F_{(2, 21)} = 33.7$]. The PS showed an opposite pattern, as it increased in the PM [$F_{(2, 21)} = 37.22$]. However, PI, PI(4)P, and PI(4,5)P2 were slightly increased and PS was decreased in the ER [Fig. 1E, PI: $F_{(2, 21)} = 10.44$; PI(4)P: $F_{(2, 21)} = 11.96$; PI(4,5)P2: $F_{(2, 21)} = 15.34$; PS: $F_{(2, 21)} = 5.10$]. PI(3,4,5)P3 was not significantly affected.

3.3. ORP5 redistributed PIs and PS between the PM and ER

Specific nonvesicular lipid transfer pathways play crucial roles in the maintenance of membrane lipid composition [11]. Therefore, we investigated the expression of ORP1A, ORP5, ORP7, and ORP8 since they have been reported to transfer PIs or PS [10]. We found that the ORP5 protein was upregulated in the injured sensorimotor cortex [$F_{(2, 21)} = 34.12$], while the other proteins were not changed (Fig. 2A). The mRNA level of ORP5 was unaltered after injury, indicating that ORP5 mRNA underwent post-transcriptional regulation (Fig. 2B).

To test the function of ORP5, we employed 4-hydroxytamoxifen (4-OH-TAM)-inducible *Cre* mice. Heterozygous *Cre* mice were crossed with an *Osbpl5* $^{fl/fl}$ transgenic line in which *loxP* sites flanked exons 8 and 9 of *Osbpl5* to produce *Osbpl5* $^{(-/-)}$ mice. After intracerebral injection of 4-OH-TAM, *Osbpl5* was specifically deleted in the sensorimotor cortex (Fig. 2C). In all cases, wild-type (WT) and heterozygous *Cre* mice (without *loxP* sites) [*Osbpl5* $^{(+/+)}$] were used as controls. Both *Osbpl5* $^{(+/+)}$ and *Osbpl5* $^{(-/-)}$ mice were injected with 4-OH-TAM to induce *Cre* expression. Fig. 2D presents the experimental process. At day 3 post-reperfusion, *Osbpl5* $^{(-/-)}$ mice showed a substantial decrease in the ORP5 protein in the sensorimotor cortex relative to injured *Osbpl5* $^{(+/+)}$ mice [Fig. 2E, $F_{(3, 28)} = 123.6$]. RT-PCR also showed that *Osbpl5* mRNA was abolished in *Osbpl5* $^{(-/-)}$ mice (Fig. 2F).

Next, the results showed that loss of ORP5 dramatically increased PI(4)P, PI(4,5)P2 and PI(3,4,5)P3 and decreased PS in the PM [Fig. 2G, PI(4)P: $F_{(3, 28)} = 29.35$; PI(4,5)P2: $F_{(3, 28)} = 20.50$; PI(3,4,5)P3: $F_{(3, 28)} = 13.41$; PS: $F_{(3, 28)} = 21.56$]. In the ER, silencing of *Osbpl5* resulted in the absence of PI, PI(4)P, and PI(4,5)P2 and the enrichment of PS in the injured sensorimotor cortex [Fig. 2H, PI: $F_{(3, 28)} = 7.18$; PI(4)P: $F_{(3, 28)} = 18.24$; PI(4,5)P2: $F_{(3, 28)} = 14.76$; PS: $F_{(3, 28)} = 7.151$]. However, PI(3,4,5)P3 was not affected by ORP5 in either the tMCAO or *Osbpl5* knockout groups. These data demonstrated that ORP5 contributes to the homeostasis of PI, PI(4)P, PI(4,5)P2 and PI(3,4,5)P3 in the sensorimotor cortex.

3.4. In vivo, decreased PI(3,4,5)P3 in the PM weakened AKT activity to induce cell damage

Induction of PI(3,4,5)P3 resulted in recruitment and activation of AKT to suppress cell apoptosis and autophagy [22,23]. Given the role of ORP5 in the transfer of PI and its derivatives, we hypothesized that ORP5 is also required during cell damage [12,13] (Fig. 3A). As shown in Fig. 3B and 3C, AKT phosphorylated at serine-473 had a negative correlation with the ORP5 level. Phosphorylated AKT (P-AKT) was decreased in WT and *Osbpl5* $^{(+/+)}$ mice after reperfusion at 3 days but increased in *Osbpl5* knockout mice [Fig. 3C, $F_{(3, 28)} = 18.34$]. Moreover, cleaved caspase-3, caspase-9, and PARP, which increase in response to AKT inactivation as apoptotic markers, were strongly increased in transient ischemia mice with ORP5 upregulation and attenuated in ORP5-deficient cortex samples [Figure 3B and 3D-3F, cleaved caspase-3: $F_{(3, 28)} = 94.02$; cleaved caspase-9: $F_{(3, 28)} = 210.2$; cleaved PARP: $F_{(3, 28)} = 119.5$]. Supplementary Fig. 2A presents the transient ischemia-elevated autophagy indicator LC3-II in both WT and *Osbpl5* $^{(+/+)}$ mice, and *Osbpl5* knockout suppressed LC3-II levels [$F_{(3, 28)} = 20.10$]. The morphological test found that the number of TUNEL-positive cells was increased in WT and *Osbpl5* $^{(+/+)}$ mice at 7 days. After knocking out *Osbpl5*, the number of positive cells was reduced in the 4-OH-TAM injection sites [Fig. 3G, $F_{(3, 28)} = 148.2$].

Next, neurobehavioural tests, including the Z-longa, modified neurological severity score (mNSS), and rotarod assessments, were performed. As shown in Fig. 3H–J, WT control mice showed no neurological deficit. There were no significant differences between the WT tMCAO and *Osbpl5* $^{(+/+)}$ tMCAO groups. Neurological damage was slightly ameliorated after injury. Notably, the neurological functional outcome significantly improved in the *Osbpl5* knockout group compared with that in the *Osbpl5* $^{(+/+)}$ group. The data were analysed by two-way ANOVA followed by a post hoc test. The significant main effects of groups were Z-longa, $F_{(3, 28)} = 82.23$, $p < 0.001$; mNSS, $F_{(3, 28)} = 52.30$, $p < 0.001$; rotarod assessments, $F_{(3, 28)} = 39.41$, $p < 0.001$. Additionally, main effects of time were also observed [Z-longa, $F_{(2, 56)} = 28.49$, $p < 0.001$; mNSS, $F_{(2, 56)} = 84.94$ $p < 0.001$; rotarod assessments, $F_{(2, 56)} = 37.01$, $p < 0.001$]. In addition, group × time interactions were observed [Z-longa, $F_{(6, 56)} = 3.80$, $p = 0.0031$; mNSS, $F_{(6, 56)} = 9.87$, $p < 0.001$; rotarod assessments, $F_{(6, 56)} = 3.96$, $p = 0.0023$]. The important significant differences were determined through a post hoc test (Tukey's multiple comparisons) are shown in Fig. 3H–J.

3.5. In vitro, ORP5 also inhibited PI(3,4,5)P3 in the PM to promote apoptosis

In human-derived SH-SY5Y cells, ORP5 expression was silenced using a chimeric adenovirus (Ad) vector expressing small hairpin (sh) RNAs of *OSBPL5*. Scrambled shRNA was used as a negative control (NC). Then, the cells were subjected to oxygen-glucose deprivation (OGD) and reoxygenation treatment. The overall expression of the ORP5 protein was upregulated in the OGD group and then downregulated after Ad infection [Supplementary Fig. 3A, $F_{(3, 16)} = 37.11$]. Consistent with the in vivo results, knockdown of ORP5 expression also resulted in the activation of AKT [Supplementary Fig. 3A, $F_{(3, 16)} = 18.77$]. Again, the number of TUNEL-positive cells was increased

in the OGD group, while silencing of ORP5 reduced the cell number (Supplementary Fig. 3B, $F_{(3,\ 16)}$ = 216.2).

We then confirmed whether ORP5 also disturbed the homeostasis of PIs in SH-SY5Y cells. In the PM, depleted PI, PI(4)P, PI(4,5)P2 and PI (3,4,5)P3 levels and increased PS levels were observed in OGD conditions. *OSBPL5* knockdown inhibited the changes in these metabolites, except for PI [Supplementary Fig. 3C, PI: $F_{(3,\ 16)}$ = 7.11; PI(4)P: $F_{(3,\ 16)}$ = 16.34; PI(4,5)P2: $F_{(3,\ 16)}$ = 19.56; PI(3,4,5)P3: $F_{(3,\ 16)}$ = 26.33; PS: $F_{(3,\ 16)}$ = 37.17]. OGD cells showed higher PI and PI(4)P levels and lower PS levels in the ER than the control cells. Silencing ORP5 reversed these alterations, which reduced PI and PI(4)P and enriched PS. Under these conditions, PI(4,5)P2 and PI(3,4,5)P3 were not significantly changed [Supplementary Fig. 3D, PI: $F_{(3,\ 16)}$ = 8.32; PI(4)P: $F_{(3,\ 16)}$ = 36.13; PS: $F_{(3,\ 16)}$ = 4.11].

3.6. The ORP5 protein elevation was regulated by miR-124-3p and miR-32-5p

MiRNAs negatively regulate gene expression by inhibiting mRNA translation. Fig. 2A and B shows the inconsistent transcription and translation levels of *Osbpl5*, which prompted us to test whether *Osbpl5* is regulated by miRNAs. RNA sequencing identified a total of 651 miRNAs in the control and tMCAO mice. In addition, 54 miRNAs were identified by de novo transcriptome assembly (Supplementary Table 1). The miRNAs that had a fold change > 2 were selected as significantly altered miRNAs. In Fig. 4A, a heatmap shows that 37 miRNAs were upregulated and 37 were downregulated in the sensorimotor cortex of tMCAO mice. Bioinformatics analysis using TargetScan [24] revealed that 277 miRNAs might bind to the *Osbpl5* mRNA. After crossing with altered miRNAs, miR-124-3p, miR-203a-5p, miR-32-5p, and miR-665 were identified as potential targets that regulate *Osbpl5* translation (Fig. 4B).

Then, stem-loop RT-PCR confirmed that miR-124-3p and miR-203a-5p were significantly enriched in the injured sensorimotor cortex and SH-SY5Y cells [Fig. 4C and D, miR-124-3p in vivo: $F_{(2,\ 21)}$ = 16.13, in vitro: $t_{(8)}$ = 8.24; miR-203a-5p in vivo: $F_{(2,\ 21)}$ = 53.07, in vitro: $t_{(8)}$ = 10.63]. Moreover, miR-32-5p and miR-665 were significantly depleted [Fig. 4C and D, miR-32-5p in vivo: $F_{(2,\ 21)}$ = 5.99, in vitro: $t_{(8)}$ = 4.36; miR-665 in vivo: $F_{(2,\ 21)}$ = 13.00, in vitro: $t_{(8)}$ = 2.95].

Next, the full-length 3′ untranslated region (UTR) of *Osbpl5* mRNA

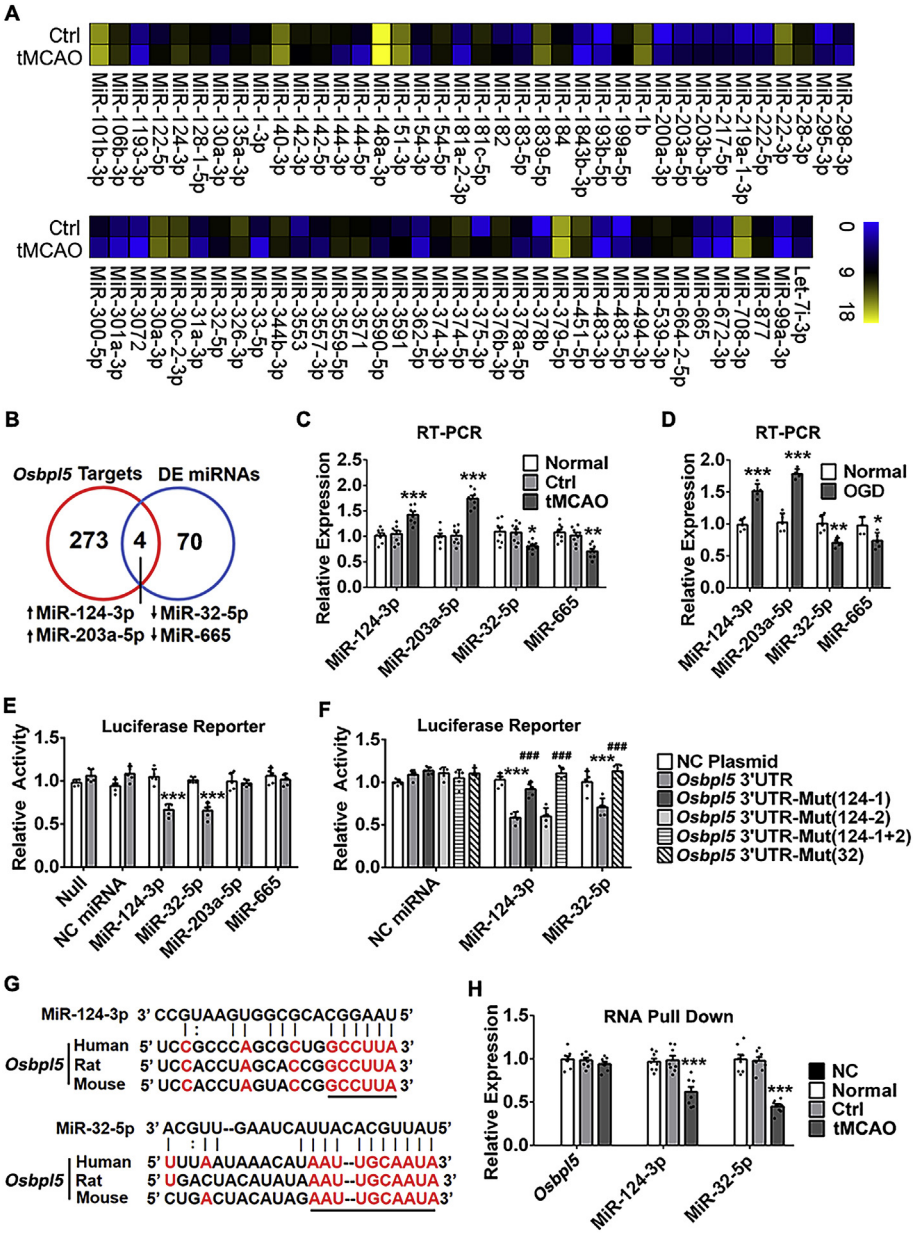

Fig. 4. After transcription, *Osbpl5* is regulated by miR-124-3p and miR-32-5p. **(A)** RNA sequencing heatmap of the 74 differentially expressed miRNAs between the control and tMCAO mice; n = 3 per group. **(B)** Four differentially expressed miRNAs were also predicted by TargetScan software as targets of the ORP5 mRNA. Two of them were increased, and the other two were reduced. **(C, D)** In mice and SH-SY5Y cells, RT-PCR confirmed that the expression of all four candidates was consistent with the sequencing results; n = 5 or 8 per group. **(E)** MiR-124-3p and miR-32-5p mimic binding to *Osbpl5-luciferase* recombinant mRNA inhibits luciferase activity; n = 5 per group. **(F)** *Osbpl5* mRNA has two miR-124-3p sites. Mutating the miR-124-3p-1 or miR-32-5p binding site can restore the mimic-inhibited luciferase activity; n = 5 per group. **(G)** miR-124-3p and miR-32-5p conservatively bind to the 3′ UTR of *Osbpl5*. Red letters indicate the conserved sequence. Vertical hyphens indicate the target of miRNAs. The underline shows the mutation in the *Osbpl5* mRNA sequence. **(H)** The antisense nucleic acid probe of *Osbpl5* mRNA was used to pull down the *Osbpl5*-miRNA complex. RT-PCR shows that miR-124-3p and miR-32-5p bind to *Osbpl5* mRNA in vivo, but this interaction is reduced after ischemia injury; NC, the probe with a random sequence; n = 8 per group. *, compared with the Ctrl or NC plasmid group; #, mutation group compared with the *Osbpl5* 3′ UTR group. (For interpretation of the references to colour in this figure legend, the reader is referred to the Web version of this article).

was cloned downstream of the *luciferase* gene in a reporter vector. The vector, in combination with miRNA mimics, was cotransfected into 293T cells. At 48 h, robust decreases in luciferase activity were observed in the miR-124-3p and miR-32-5p groups [Fig. 4E, main effects of miRNAs, $F_{(5, 48)} = 13.93$, $p < 0.001$; main effects of plasmid, $F_{(1, 48)} = 25.00$, $p < 0.001$; and miRNA × plasmid interactions, $F_{(5, 48)} = 21.54$, $p < 0.001$].

Sequence analysis further predicted that miR-124-3p had 2 binding sites and that miR-32-5p had 1 binding site in the *Osbpl5* 3′ UTR. Accordingly, point mutations were introduced into the WT *Osbpl5* 3′ UTR to abolish the predicted seed pairing of miR-124-3p and miR-32-5p. Compared with the WT group, the miR-124-3p mutant-1, miR-124-3p mutant-1 + 2, and miR-32-5p groups showed restored luciferase activity. However, the miR-124-3p mutant-2 group did not show significantly recovered luciferase activity. Two-way ANOVA showed the main effects of miRNAs [$F_{(2, 72)} = 102.50$, $p < 0.001$] and the plasmid [$F_{(5, 72)} = 16.39$, $p < 0.001$]. The miRNA × plasmid interactions were also examined [$F_{(10, 72)} = 26.72$, $p < 0.001$] (Fig. 4F). These results suggested that the repressive effect of miR-124-3p and miR-32-5p on the WT *Osbpl5* 3′ UTR was mediated via a single, highly conserved binding site (Fig. 4G).

Interestingly, both the ORP5 protein and miR-124-3p were upregulated after injury (Figs. 2A, 4C and 4D and Supplementary Fig. 3A). In theory, these molecules should be negatively regulated. To explore this conflict, the sensorimotor cortex was lysed and incubated with *Osbpl5* mRNA-specific or nonspecific (NC) nucleic acid probes and then harvested with streptavidin beads. After normalization to the housekeeping genes in the input samples, the RT-PCR results indicated that the probe-enriched *Osbpl5* mRNA showed no significant differences among the groups, which was consistent with the *Osbpl5* mRNA expression (Figs. 2B and 4H). Strikingly, the *Osbpl5* probe showed a significantly reduced ability to pull down miR-124-3p and miR-32-5p in the tMCAO group with ORP5 protein upregulation, indicating that the interaction between *Osbpl5* and miR-124-3p or miR-32-5p exists in vivo [Fig. 4H, miR-124-3p: $F_{(3, 28)} = 122.00$; miR-32-5p: $F_{(3, 28)} = 169.20$]. Therefore, miR-124-3p and miR-32-5p were responsible for the post-transcriptional regulation of *Osbpl5*.

3.7. Hsa_circ_0001449 sponged miR-124-3p and miR-32-5p to promote Osbpl5 expression in SH-SY5Y cells

The total miR-124-3p level was strongly increased after transient

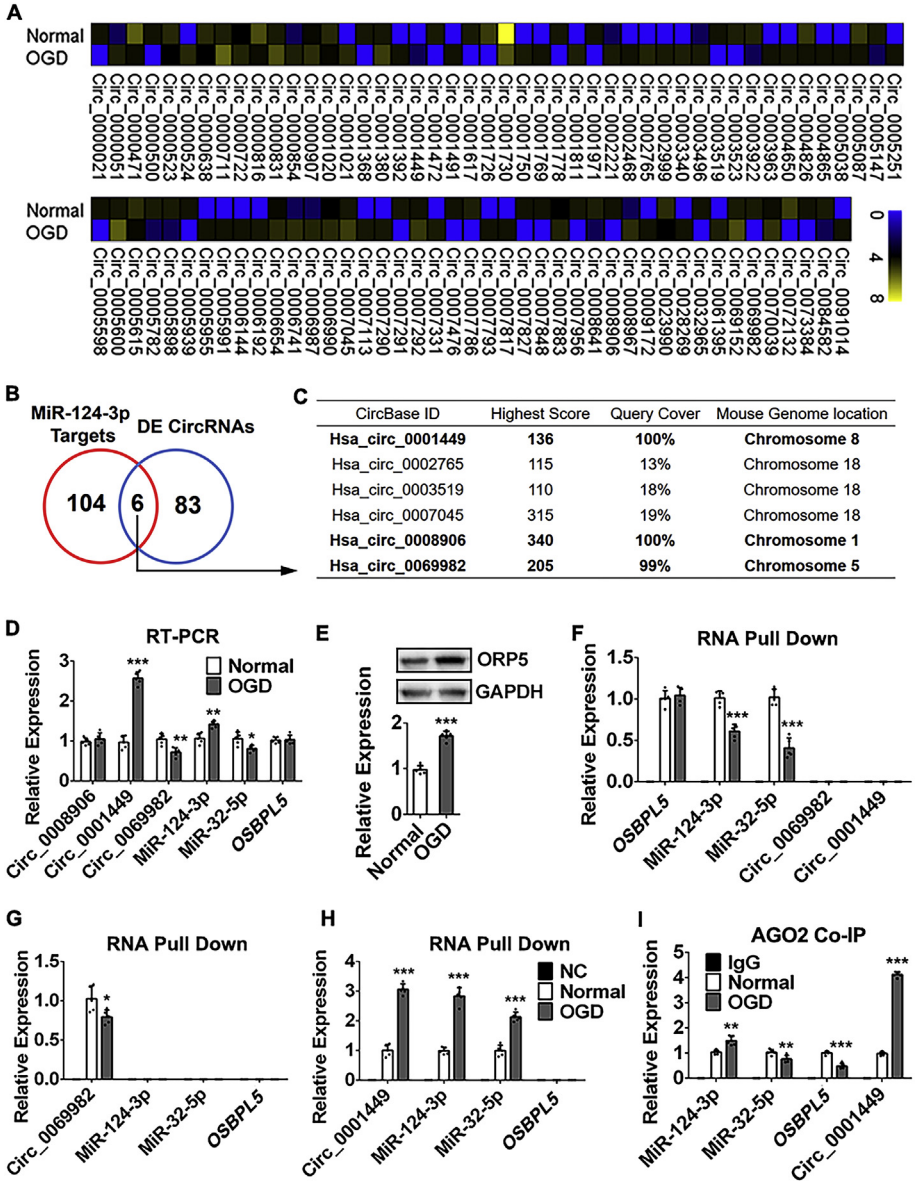

Fig. 5. Hsa_circ_0001449 sponges miR-124-3p and miR-32-5p to release *Osbpl5* translation from miRNA inhibition. **(A)** CircRNA sequencing heatmap showing 89 differentially expressed circRNAs in oxygen-glucose deprivation (OGD)-treated human SH-SY5Y cells; n = 3 per group. **(B)** Six differentially expressed circRNAs were also predicted by miRanda software as targets of miR-124-3p. **(C)** Compared with the mouse genome, hsa_circ_0001449, hsa_circ_0008906, and hsa_circ_0069982 are highly conserved. **(D)** RT-PCR confirmed that hsa_circ_0001449 was sharply enriched and that hsa_circ_0069982 was decreased in the OGD group. These findings are consistent with the sequencing results; n = 5 per group. **(E)** The ORP5 protein was upregulated after OGD treatment; n = 5 per group. **(F)** The antisense probe for *OSBPL5* mRNA was used to pull down the *OSBPL5*-miRNA complex. RT-PCR showed that miR-124-3p and miR-32-5p bind to *OSBPL5* mRNA in SH-SY5Y cells, and this interaction was reduced in the OGD group. Hsa_circ_0001449 and hsa_circ_0069982 did not bind to *OSBPL5* mRNA. n = 5 per group; NC, the probe with a random sequence. **(G)** The hsa_circ_0069982 probe only enriched hsa_circ_0069982, and it decreased in the OGD group; n = 5 per group. **(H)** The hsa_circ_0001449 probe-enriched hsa_circ_0001449, miR-124-3p and miR-32-5p but not *OSBPL5* mRNA. miR-124-3p and miR-32-5p were increased as hsa_circ_0001449 was elevated; n = 5 per group. **(I)** An anti-ago2 antibody co-immunoprecipitated (co-IP) the miRNA silencing complex. RT-PCR of the precipitated samples showed abundant hsa_circ_0001449 but low *OSBPL5* mRNA binding to the silencing complex after OGD treatment; n = 5 per group; IgG, the antibody control group. *, compared with the normal group.

ischemia (Fig. 4C and 4D), while its binding with *Osbpl5* mRNA was inhibited (Fig. 4H). Given that non-coding RNAs can regulate miRNAs, we hypothesized that circRNAs might endogenously compete with *Osbpl5* mRNA to sponge miR-124-3p. We then sought to explore their expression profiles using human SH-SY5Y cells. After intersection of the circRNA sequencing results and the circBase database, we identified 3070 circRNAs in the normal and OGD groups (Supplementary Table 2). Subsequently, circRNAs with a fold change > 2 were identified as differentially expressed circRNAs. As shown in Fig. 5A, there were 50 upregulated and 39 downregulated circRNAs in the OGD-treated cells.

Next, the miRanda online tool predicted that 110 circRNAs may bind to miR-124-3p [25]. After assessing the intersection with differentially expressed circRNAs, 6 circRNAs were subjected to sequential conservation analysis (Fig. 5B). Hsa_circ_0001449, hsa_circ_0008906, and hsa_circ_0069982 were identified as highly conserved potential targets (Fig. 5C).

Next, qRT-PCR confirmed that hsa_circ_0001449 [$t_{(8)}$ = 15.61] and hsa_circ_0069982 [$t_{(8)}$ = 4.24] were strongly correlated with the sequencing results (Fig. 5D). In addition, miR-124-3p was upregulated [$t_{(8)}$ = 4.91], miR-32-5p was downregulated [$t_{(8)}$ = 3.01], and *OSBPL5* mRNA was unchanged in the OGD group (Fig. 5D). The ORP5 protein was upregulated [$t_{(8)}$ = 11.64] in SH-SY5Y cells (Fig. 5E). These data were consistent with the in vivo results (Fig. 2A, 2B and 4C).

Furthermore, qRT-PCR showed that *OSBPL5* mRNA, miR-124-3p, and miR-32-5p were successfully pulled down by the *OSBPL5* probe in vitro. However, hsa_circ_0001449 and hsa_circ_0069982 were not detected, which indicated that they did not directly interact with *OSBPL5*. After OGD treatment, the *OSBPL5* mRNA probe-enriched miR-124-3p and miR-32-5p were significantly decreased [Fig. 5F, miR-124-3p, $t_{(8)}$ = 7.72; miR-32-5p, $t_{(8)}$ = 8.80], which was consistent with the previous in vivo results (Fig. 4H). When the hsa_circ_0069982 probe was used, the OGD group showed depleted hsa_circ_0069982 binding [Fig. 5G, $t_{(8)}$ = 2.80]. However, miR-124-3p and miR-32-5p were not detected, indicating that hsa_circ_0069982 did not contribute to ORP5 function (Fig. 5G). Excitingly, the hsa_circ_0001449 probe data indicated that hsa_circ_0001449 could competitively sponge miR-124-3p and miR-32-5p. In the OGD group, miR-124-3p and miR-32-5p pulled down by the hsa_circ_0001449 probe were elevated, as was hsa_circ_0001449 [Fig. 5H, hsa_circ_0001449, $t_{(8)}$ = 17.07; miR-124-3p, $t_{(8)}$ = 13.87; miR-32-5p, $t_{(8)}$ = 10.33].

Ago2 is the catalytic centre of the RNA-induced silencing complex [26]. Ago2 immunoprecipitation using SH-SY5Y cells found that miR-124-3p and miR-32-5p bound to Ago2 were increased and decreased, respectively, in the OGD group [miR-124-3p, $t_{(8)}$ = 4.92; miR-32-5p, $t_{(8)}$ = 3.41]. Notably, the enriched hsa_circ_0001449 was increased after OGD treatment, while *OSBPL5* mRNA was reduced (Fig. 5I, hsa_circ_0001449, $t_{(8)}$ = 53.27; *OSBPL5*, $t_{(8)}$ = 9.01).

Next, using the recombinant hsa_circ_0001449-*luciferase* plasmid, we showed that miR-124-3p and miR-32-5p had inhibitory effects on

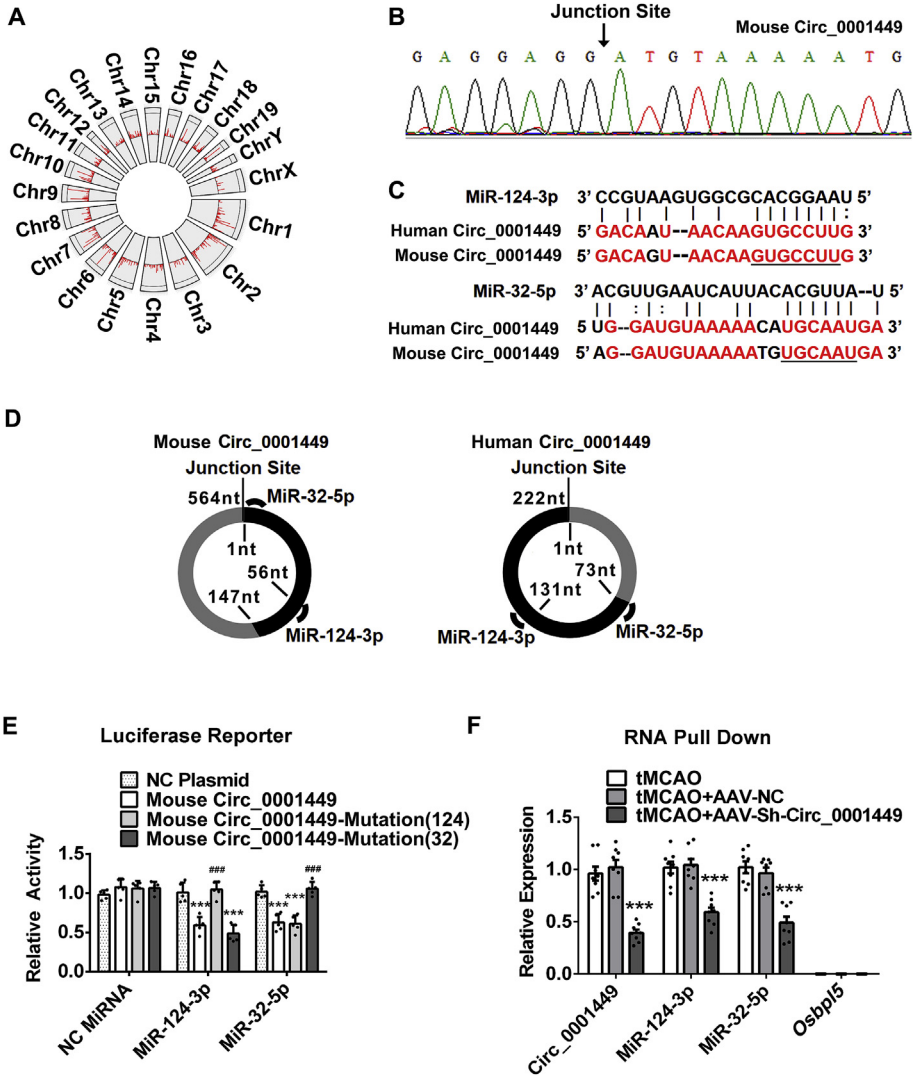

Fig. 6. Circ_0001449 also exists in the mouse sensorimotor cortex and pairs with miR-124-3p and miR-32-5p. (A) Circos present the distribution of identified mouse circRNAs in chromosomes. **(B)** Pyrosequencing verifies the junction site of a conservative de novo circRNA. **(C)** The miR-124-3p and miR-32-5p binding sites in human and mouse circ_0001449 are highly conserved. Red letters indicate the conserved sequence. Vertical hyphens indicate the targets of miRNAs. The underline shows the mutation of the circ_0001449 sequence used in the luciferase reporter assay. **(D)** Schematic of the mouse and human circ_0001449 structure displaying the miR-124-3p and miR-32-5p binding sites and the junction sites. The mouse circ_0001449 has a total of 564 bases, and human circ_0001449 has a total of 222 bases. The dark area indicates the conserved sequence. **(E)** MiR-124-3p and miR-32-5p mimic binding to the mouse circ_0001449-*luciferase* recombinant RNA inhibits luciferase activity. In addition, mutating the miR-124-3p or miR-32-5p binding site can restore the mimic-inhibited luciferase activity; n = 5 per group. **(F)** In tMCAO mice, RT-PCR was used to assess the pull down samples. The circ_0001449 probe enriched circ_0001449, miR-124-3p and miR-32-5p but not *Osbpl5* mRNA. miR-124-3p and miR-32-5p were decreased when circ_0001449 was downregulated by adeno-associated virus (AAV); n = 8 per group. *, compared with the NC plasmid or tMCAO + AAV-NC group; #, mutation group compared with the mouse circ_0001449 group. (For interpretation of the references to colour in this figure legend, the reader is referred to the Web version of this article).

the luciferase activity. In the miR-124-3p treatment groups, the luciferase activity was recovered when the miR-124-3p binding sites were mutated in the circRNAs, and no effects were observed when the miR-32-5p binding sites were mutated. In the miR-32-5p treatment groups, the luciferase activity was also specifically recovered when the miR-32-5p binding sites were mutated. Two-way ANOVA showed the main effects of the miRNAs [$F_{(2, 48)} = 17.51$, $p < 0.001$], the plasmid [$F_{(3, 48)} = 15.24$, $p < 0.001$], and the miRNA × plasmid interactions [$F_{(6, 48)} = 12.24$, $p < 0.001$] (Supplementary Fig. 4A).

Taken together, these results demonstrated our hypothesis that hsa_circ_0001449 sponges miR-124-3p and miR-32-5p from ORP5 mRNA after injury. This process blocked the effects of miR-124-3p and miR-32-5p, even though miR-124-3p was upregulated.

3.8. Circ_0001449 conservatively paired with miR-124-3p and miR-32-5p in both humans and mice

We further investigated whether circ_0001449 also existed in mice. First, we used RNA sequencing to identify the circRNA junction site in the mouse sensorimotor cortex. Fig. 6A presents the distribution of identified circRNAs in chromosomes. A de novo circRNA showed a highly conserved sequence with hsa_circ_0001449 that contained both miR-124-3p and miR-32-5p binding sites. The full-length sequence information of human and mouse circ_0001449 is shown in Supplementary Fig. 5A. Next, we designed primers that were located across the junction site of mouse circ_0001449 (Supplementary Table 3). After specific RT-PCR amplification, pyrosequencing verified the junction site sequence of mouse circ_0001449 (Fig. 6B). Fig. 6C further shows that miR-124-3p and miR-32-5p had highly matched sequences with human or mouse circ_0001449. Finally, a schematic diagram representing the mouse and human circ_0001449 structure is shown in Fig. 6D.

Next, the luciferase reporter assay found that the mouse circ_0001449 recombinant *luciferase* plasmid inhibited the luciferase activity by miR-124-3p and miR-32-5p. Next, in the miR-124-3p or miR-32-5p treatment groups, the luciferase activity was specifically recovered when the miR-124-3p or miR-32-5p binding site was mutated. Two-way ANOVA showed the main effects of miRNAs [$F_{(2, 48)} = 39.61$, $p < 0.001$], the plasmid [$F_{(3, 48)} = 14.47$, $p < 0.001$], and the miRNA × plasmid interactions [$F_{(6, 48)} = 28.56$, $p < 0.001$] (Fig. 6E).

The biotin-labelled mouse circ_0001449 nucleic acid probe was used to pull down the circ_0001449 complex in the sensorimotor cortex. Moreover, an adeno-associated virus (AAV) was adopted to down-regulate circ_0001449 expression (Supplementary Figs. 5B and 5C). As shown in Fig. 6F, circ_0001449 was pulled down by its probe and decreased after AAV injection [$F_{(2, 21)} = 34.64$]. As expected, *Osbpl5* was not pulled down by the probe. In addition, miR-32-5p and miR-124-3p displayed strong binding to circ_0001449. After suppression of circ_0001449, miR-32-5p and miR-124-3p were significantly depleted [Fig. 6F, miR-32-5p: $F_{(2, 21)} = 26.79$; miR-124-3p: $F_{(2, 21)} = 22.65$]. These results suggested that circ_0001449 also regulated miR-32-5p and miR-124-3p in mice.

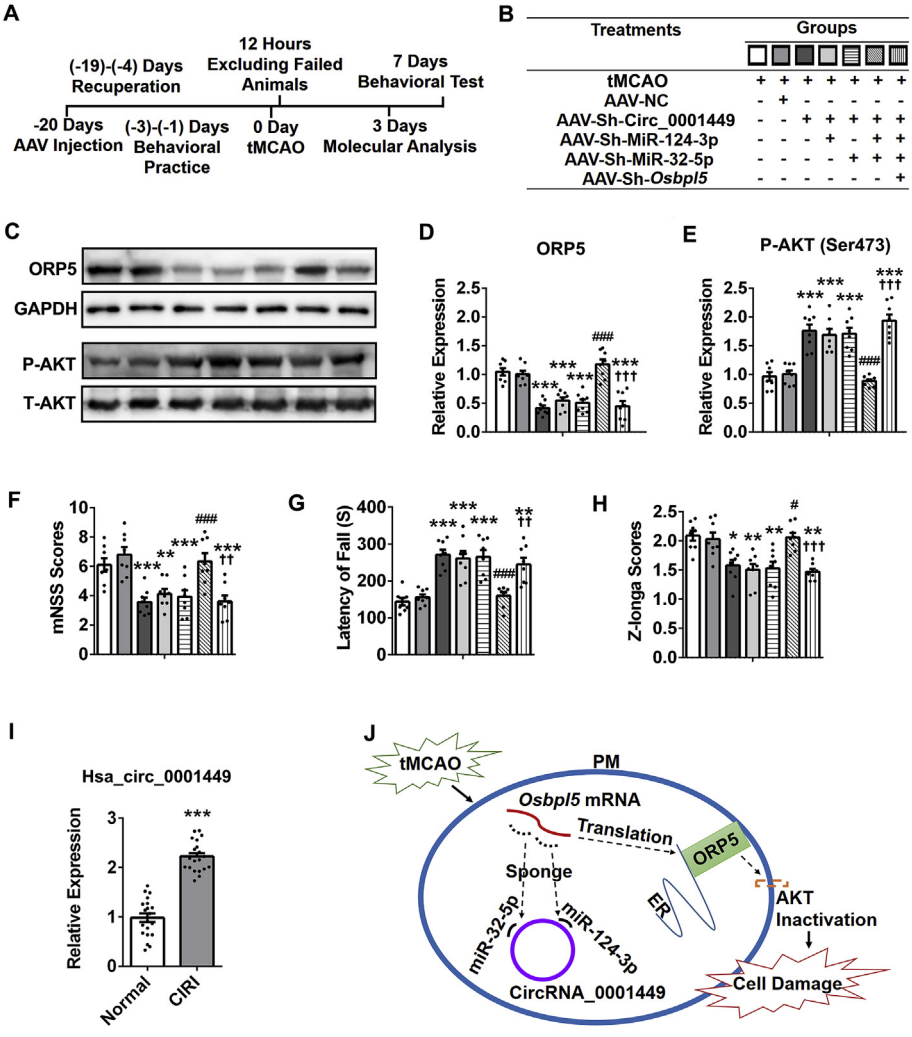

Fig. 7. The rescue and block experiments in tMCAO mice confirmed the regulation of circ_0001449, miR-124-3p/miR-32-5p, and the ORP5 axis. (A) Illustration of the experimental procedure using AAV to knock down multiple RNAs in the sensorimotor cortex. **(B)** Diagram of the mouse groups and treatments. **(C–E)** Immunoblotting reveals that the expression of OPR5 and the activity of P-AKT are regulated by a series of effects on circ_0001449, miR-124-3p, miR-32-5p and OPR5; n = 8 per group. **(F–H)** The variation in neurobehaviour was determined by Z-longa, mNSS, and rotarod tests 7 days after reperfusion; these changes were closely associated with AAV regulation; n = 8 per group. **(I)** The blood plasma of ischemia patients presented with a high level of hsa_circ_0001449; n = 20 per group. **(J)** Cartoon represents the mechanism by which circ_0001449 regulates AKT activity via miR-124-3p/miR-32-5p and ORP5. Circ_0001449 competes with *Osbpl5* mRNA to sponge miR-124-3p and miR-32-5p in ischemic mice. This process releases miR-124-3p and miR-32-5p from *Osbpl5* mRNA, which enhances the *Osbpl5* translation level. The upregulated ORP5 decreases PI(3,4,5)P3 in the PM, which impairs PI(3,4,5)P3 recruitment and activation of AKT. Finally, AKT inactivation accelerates cell damage after cerebral ischemia injury. *, compared with the tMCAO + AAV-Sh-NC group; #, compared with the tMCAO + AAV-Sh-Circ_0001449 group; †, compared with the tMCAO + AAV-Sh-Circ_0001449 + AAV-Sh-MiR-124-3p + AAV-Sh-MiR-32-5p group.

3.9. Confirmation of the circ_0001449-miR-124-3p/miR-32-5p-ORP5 axis in vivo

Given that the ORP5 protein and circ_0001449 were increased after injury (Figs. 2A and 5D), we hypothesized that circ_0001449 suppression by AAV might lead to the release of miR-32-5p and miR-124-3p from circ_0001449 and to inhibition of *Osbpl5* translation. Then, downregulated miR-32-5p and miR-124-3p might increase *Osbpl5* translation. Finally, *Osbpl5* sh-AAV decreased *Osbpl5* expression. The group treatments are shown in Fig. 7B and Supplementary Fig. 5B. The experimental process is also shown in Fig. 7A.

First, RT-PCR results demonstrated that AAV regulation was successful in the mouse sensorimotor cortex at 3 days after tMCAO [Supplementary Fig. 5C, circ_0001449, $F_{(6,\ 49)} = 17.86$; miR-124-3p, $F_{(6,\ 49)} = 26.32$; miR-32-5p, $F_{(6,\ 49)} = 47.27$; ORP5, $F_{(6,\ 49)} = 16.14$]. Second, we examined the protein expression of ORP5 [Fig. 7C and 7D, $F_{(6,\ 49)} = 23.84$]. In the sensorimotor cortices of the tMCAO mice, compared with AAV-sh-NC administration, AAV-sh-circ_0001449 administration successfully suppressed the ORP5 protein levels. However, separate AAV-sh-miR-124-3p or AAV-sh-miR-32-5p injections could not block the effect of AAV-sh-circ_0001449. Only coadministration could significantly rescue the ORP5 level. Further AAV-sh-*Osbpl5* treatment decreased the ORP5 levels. Finally, Fig. 7C and 7E shows that the AKT activity presented an opposite pattern from that of ORP5 with the AAV treatments [$F_{(6,\ 49)} = 25.26$]. Therefore, circ_0001449-sponged miR-124-3p and miR-32-5p might contribute to the apoptosis and autophagy induced by ORP5 and AKT.

Furthermore, AAV-sh-circ_0001449 induced a recovery of the mNSS [Fig. 7F–H, $F_{(6,\ 49)} = 10.50$], rotarod assessments [$F_{(6,\ 49)} = 15.53$], and Z-longa [$F_{(6,\ 49)} = 9.66$] at 7 days. AAV-sh-miR-124-3p and AAV-sh-miR-32-5p coinjection successfully impaired AAV-sh-circ_0001449 function, but a separate injection had no significant effects. Moreover, ORP5 knockdown by AAV-sh-*Osbpl5* significantly improved the neurological functional outcome. These data emphasized that circ_0001449 has a strong correlation with the neurobehaviour of tMCAO mice. Finally, the cerebral ischemia patient plasma samples also showed an increased circ_0001449 level [Fig. 7I, $t_{(38)} = 11.16$], indicating that circ_0001449 may be a potential biomarker in ischemic injury.

4. Discussion

Membrane organelles dynamically maintain homeostasis and adjust based on the various needs of the cell. Some changes occur as part of the normal cell cycle, and other changes occur in response to challenges or survival stress [27]. The PM and ER can participate in cell death/survival signalling pathways. Nonvesicular lipid transfer between the membranes of different organelles is now recognized as a major contributor to membrane homeostasis [10]. Our data expanded the function of the lipid transport protein ORP5 in cerebral ischemia injury. This protein transports PI(4)P or PI(4,5)P2 from the PM to the ER, which eliminates the PI(3,4,5)P3 source of the PM. Additionally, circ_0001449 sponges miR-124-3p and miR-32-5p to abolish the translational suppression of *Osbpl5*. Upregulated ORP5 decreases PI(3,4,5)P3 in the PM, which impairs PI(3,4,5)P3 recruitment and AKT activation. Finally, this molecule accelerates cell apoptosis and autophagy after injury (Fig. 7J).

4.1. Circ_0001449 and ORP5 may play a role in ischemic induced cerebral oxidative injury

Cerebral ischemic results in energy failure that initiates a complex series of metabolic events, ultimately causing cell damage. One such critical event is oxidative injury [2]. In the present study, circ_0001449 and ORP5 decreased AKT activity after cerebral ischemic. AKT has been reported to weaken reactive oxygen species-induced cell injury [28–30]. For instance, AKT enhanced Nrf2 activation to attenuate apoptosis. Nrf2 regulates basal and inducible transcription of genes encoding molecules that protect against various oxidative stresses [30]. Moreover, we also found that circ_0001449 sponged miR-124-3p to abolish its function. Previous studies have shown that miR-124-3p has a protective role by reducing oxidant stress and preventing cell apoptosis and autophagy, which are also involved in the Nrf2 pathway [31,32]. Therefore, we indicate that inhibiting circ_0001449 and ORP5 may have an antioxidant effect in cerebral ischemic.

4.2. ORP5 may transport one or both of PI(4)P and PI(4,5)P2

OSBP and its related protein homologs, ORPs, constitute a conserved family of LTPs that are ubiquitously expressed in eukaryotes. Phosphorylated PI serves as an essential signalling molecule at the PM. Most ORPs carry targeting determinants for ER and non-ER organelle membranes [10]. Chung et al. recently reported that ORP5 and ORP8 could mediate PI(4)P/PS transport between the ER and the PM, thus delivering PI(4)P to the ER-localized PI(4)P phosphatase SAC1 for degradation and PS from the ER to the PM [12]. However, a contradictory result showed that knocking down both ORP5 and ORP8 had little effect on the PM level of PI(4)P but dramatically increased the PM level of PI(4,5)P2[13]. Moreover, the lipid transport activity depended on the levels of both PI(4)P and PI(4,5)P2 within the PM [15]. In the present study, only ORP5 was upregulated by tMCAO injury. Both PI(4)P and PI(4,5)P2 were increased in the PM and decreased in the ER after knocking out *Osbpl5* in the mouse sensorimotor cortex (Fig. 2G and 2H). In contrast to the results in mice, PI(4,5)P2 of human SH-SY5Y cells did not show any regulation in the ER, although other alterations were similar to those in the mouse data (Supplementary Figs. 3C and 3D). This finding indicates that ORP5 may transport PI(4)P and PI(4,5)P2 in the mouse sensorimotor cortex but only transports PI(4)P in human SH-SY5Y cells. As shown in Fig. 3A, PI(4)P in the ER is hydrolysed by SAC1 to form PI, but in the PM, it is phosphorylated by PIP5K to form PI(4,5)P2[14, 16]. Therefore, the altered PI(4,5)P2 in the PM of SH-SY5Y cells may be due to its precursor, PI(4)P, which is affected by ORP5 transport. Thus, we suggest that ORP5 may deliver both PI(4)P and PI(4,5)P2 or only PI(4)P depending on the different species or cell types. The underlying regulatory mechanism of this difference requires further exploration.

4.3. After cerebral ischemia, upregulated ORP5 may contribute to the deficit of inositol 1,4,5-trisphosphate (IP3)

As shown in Fig. 3A, PI is successively phosphorylated by PI4K, PIP5K, and PI3K to yield PI(3,4,5)P3 in the PM [16]. In addition to PI3K, PI(4,5)P2 can be hydrolysed by phosphoinositide phospholipase C (PLC) to form diacylglycerol (DAG) and inositol 1,4,5-trisphosphate (IP3). IP3 is a second messenger molecule that has a complex role in various processes, including cell survival and other intracellular signalling cascades via its different receptors [33,34]. For instance, IP3 binds to its receptor to mediate Ca^{2+} release from the ER and is effectively delivered to the mitochondrial matrix to regulate oxidative metabolism and cell survival and trigger apoptosis [35,36].

The roles of IP3 and its receptor in cerebral ischemia are still controversial. Zheng et al. reported that ischemic mice deficient in the IP3 receptor exhibited aggravated damage [37]. However, another study showed that IP3 receptor knockout mice exhibited less neuronal apoptosis and tissue loss than wild-type mice [38]. Moreover, previous reports have shown a weakened IP3 receptor [39–41]. IP3 also showed a significant deficit after cerebral ischemia [42–45], and PLC was not upregulated [42,46]. In this study, Figs. 1D and Fig. 2G show that ORP5 induced a decrease in PI(4,5)P2 in the PM. We suggest that this low level of PI(4,5)P2 may result in a deficit in IP3 levels. In future studies, we will clarify whether ORP5 plays a role in IP3 signalling.

4.4. The phosphorylated PI in the PM and ER may undergo different metabolic processes

PI(3,4,5)P3 is generated by the phosphorylation of PI through a series of reactions involving phosphoinositide kinases, including PI4K, PIP5K, and PI3K[16]. Increasing evidence suggests that they primarily react at the PM [47–50]. For example, a high-sensitivity biosensor for PI(3,4)P2 has shown that PI3K produces PI(3,4,5)P3 in the PM [48]. PIP5K was found to be indispensable for the production of PI(4,5)P2 in the PM to maintain cell morphogenesis [49]. In Fig. 2G, PI, the precursor of PI(4)P and PI(4,5)P2, was decreased in tMCAO mice with ORP5 elevation. Abolishing ORP5 rescued the PI(3,4,5)P3 level but did not significantly increase the PI level. This finding indicates that PI(4)P and PI(4,5)P2 in the PM are preferentially supplied to form PI(3,4,5)P3 via a series of phosphoinositide kinases.

However, Fig. 2H shows that PI was enriched in the ER because ORP5 was elevated after injury, and abolishing ORP5 decreased the PI level. Notably, PI(3,4,5)P3 did not show a significant change with ORP5 upregulation or downregulation. In the ER, SAC1 catalyses P(4)P dephosphorylation to produce PI, and inhibition of SAC1 causes accumulation of P(4)P in the ER [51]. We assume, in contrast to the results in the PM, that PI(4)P and PI(4,5)P2 preferentially yield PI in the ER. Therefore, the different distribution of enzymes may lead to the differences in phosphorylated PI between the PM and ER.

4.5. MiR-124-3p is abundant in the brain and plays important roles in stroke

The abundance of miR-124-3p in the central nervous system is more than 100 times higher than that in other organs [52]. This molecule has therapeutic potential against stroke, and the mechanisms involved are still being explored [53–55]. For example, miR-124-3p injection resulted in significantly increased neuronal survival and a significantly increased number of M2-like polarized microglia/macrophages [53]. Additionally, several studies have shown that miR-124-3p was upregulated in the middle cerebral artery occlusion (MCAO) model [54,55]. We also found that miR-124-3p was increased in the sensorimotor cortex after transient ischemia. However, the increased circ_0001449 sponged miR-124-3p, which abolished the protective function of miR-124-3p. Our results presented a novel mechanism in which circ_0001449 competed with *Osbpl5* mRNA to bind to miR-124-3p and miR-32-5p. *Osbpl5,* the target of miR-124-3p and miR-32-5p, mediates the homeostasis of phosphorylated PI between the PM and ER. Finally, ischemic stroke triggers complicated molecular events, and non-coding RNAs may replace single gene therapies in future treatments.

Sources of funding

This work was supported by the National Natural Science Foundation for Young Scientists of China, No. 81601058 (to W. L.); the Basic Research and Frontier Science Exploration Foundation of Yuzhong District, Chongqing, China, No. 20180106 (to F. F. S.); the National Natural Science Foundation of China, No. 81860234 (to X. H.) and No. 81960219 (to X. L. M.); and the Science and Technology Foundation of Guizhou Health and Family Planning Commission, Guizhou, China, No. gzwjkj2018-1-018 (to X. H.).

Declaration of competing interest

None.

Transparency document

Transparency document related to this article can be found online at https://doi.org/10.1016/j.redox.2020.101459

Appendix A. Supplementary data

Supplementary data to this article can be found online at https://doi.org/10.1016/j.redox.2020.101459.

References

[1] G. Kaidonis, A.N. Rao, Y.B. Ouyang, C.M. Stary, Elucidating sex differences in response to cerebral ischemia: immunoregulatory mechanisms and the role of micrornas, Prog. Neurobiol. 176 (2019) 73–85.
[2] D. Yuan, C. Liu, B. Hu, Dysfunction of membrane trafficking leads to ischemia-reperfusion injury after transient cerebral ischemia, Transl. Stroke Res. 9 (2018) 215–222.
[3] E. Szegezdi, S.E. Logue, A.M. Gorman, A. Samali, Mediators of endoplasmic reticulum stress-induced apoptosis, EMBO Rep. 7 (2006) 880–885.
[4] Y. Cai, J. Arikkath, L. Yang, M.L. Guo, P. Periyasamy, S. Buch, Interplay of endoplasmic reticulum stress and autophagy in neurodegenerative disorders, Autophagy 12 (2016) 225–244.
[5] M. Niu, X. Dai, W. Zou, X. Yu, W. Teng, Q. Chen, X. Sun, W. Yu, H. Ma, P. Liu, Autophagy, endoplasmic reticulum stress and the unfolded protein response in intracerebral hemorrhage, Transl. Neurosci. 8 (2017) 37–48.
[6] A.M. Cuervo, The plasma membrane brings autophagosomes to life, Nat. Cell Biol. 12 (2010) 735–737.
[7] K. Moreau, D.C. Rubinsztein, The plasma membrane as a control center for autophagy, Autophagy 8 (2012) 861–863.
[8] Y. Zhang, X. Chen, C. Gueydan, J. Han, Plasma membrane changes during programmed cell deaths, Cell Res. 28 (2018) 9–21.
[9] R. Behnia, S. Munro, Organelle identity and the signposts for membrane traffic, Nature 438 (2005) 597–604.
[10] H. Kentala, M. Weber-Boyvat, V.M. Olkkonen, Osbp-related protein family: mediators of lipid transport and signaling at membrane contact sites, Int. Rev. Cell Mol. Biol. 321 (2016) 299–340.
[11] W.A. Prinz, Bridging the gap: membrane contact sites in signaling, metabolism, and organelle dynamics, J. Cell Biol. 205 (2014) 759–769.
[12] J. Chung, F. Torta, K. Masai, L. Lucast, H. Czapla, L.B. Tanner, P. Narayanaswamy, M.R. Wenk, F. Nakatsu, P. De Camilli, Intracellular transport. Pi4p/phosphatidylserine countertransport at orp5- and orp8-mediated er-plasma membrane contacts, Science 349 (2015) 428–432.
[13] R. Ghai, X. Du, H. Wang, J. Dong, C. Ferguson, A.J. Brown, R.G. Parton, J.W. Wu, H. Yang, Orp5 and orp8 bind phosphatidylinositol-4, 5-biphosphate (ptdins(4,5)p 2) and regulate its level at the plasma membrane, Nat. Commun. 8 (2017) 757.
[14] C.J. Stefan, A.G. Manford, D. Baird, J. Yamada-Hanff, Y. Mao, S.D. Emr, Osh proteins regulate phosphoinositide metabolism at er-plasma membrane contact sites, Cell 144 (2011) 389–401.
[15] M. Sohn, M. Korzeniowski, J.P. Zewe, R.C. Wills, G.R.V. Hammond, J. Humpolickova, L. Vrzal, D. Chalupska, V. Veverka, G.D. Fairn, E. Boura, T. Balla, Pi(4,5)p2 controls plasma membrane pi4p and ps levels via orp5/8 recruitment to er-pm contact sites, J. Cell Biol. 217 (2018) 1797–1813.
[16] Y. Liu, V.A. Bankaitis, Phosphoinositide phosphatases in cell biology and disease, Prog. Lipid Res. 49 (2010) 201–217.
[17] J.R. Hart, P.K. Vogt, Phosphorylation of akt: a mutational analysis, Oncotarget 2 (2011) 467–476.
[18] S.P. Barrett, P.L. Wang, J. Salzman, Circular rna biogenesis can proceed through an exon-containing lariat precursor, eLife 4 (2015) e07540.
[19] W. Liu, C. Jia, L. Luo, H.L. Wang, X.L. Min, J.H. Xu, L.Q. Ma, X.M. Yang, Y.W. Wang, F.F. Shang, Novel circular rnas expressed in brain microvascular endothelial cells after oxygen-glucose deprivation/recovery, Neural Regen. Res. 14 (2019) 2104–2111.
[20] B. Han, Y. Zhang, Y. Zhang, Y. Bai, X. Chen, R. Huang, F. Wu, S. Leng, J. Chao, J.H. Zhang, G. Hu, H. Yao, Novel insight into circular rna hectd1 in astrocyte activation via autophagy by targeting mir142-tiparp: implications for cerebral ischemic stroke, Autophagy 14 (2018) 1164–1184.
[21] F. Wu, B. Han, S. Wu, L. Yang, S. Leng, M. Li, J. Liao, G. Wang, Q. Ye, Y. Zhang, H. Chen, X. Chen, M. Zhong, Y. Xu, Q. Liu, J.H. Zhang, H. Yao, Circular rna tlk1 aggravates neuronal injury and neurological deficits after ischemic stroke via mir-335-3p/tiparp, J. Neurosci. (2019).
[22] Y. Yuan, Q. Guo, Z. Ye, X. Pingping, N. Wang, Z. Song, Ischemic postconditioning protects brain from ischemia/reperfusion injury by attenuating endoplasmic reticulum stress-induced apoptosis through pi3k-akt pathway, Brain Res. 1367 (2011) 85–93.
[23] R.C. Wang, Y. Wei, Z. An, Z. Zou, G. Xiao, G. Bhagat, M. White, J. Reichelt, B. Levine, Akt-mediated regulation of autophagy and tumorigenesis through beclin 1 phosphorylation, Science 338 (2012) 956–959.
[24] V. Agarwal, G.W. Bell, J.W. Nam, D.P. Bartel, Predicting effective microrna target sites in mammalian mrnas, eLife 4 (2015).
[25] B. John, A.J. Enright, A. Aravin, T. Tuschl, C. Sander, D.S. Marks, Human microrna targets, PLoS Biol. 2 (2004) e363.
[26] S.W. Chi, J.B. Zang, A. Mele, R.B. Darnell, Argonaute hits-clip decodes microrna-mrna interaction maps, Nature 460 (2009) 479–486.
[27] R. Heald, O. Cohen-Fix, Morphology and function of membrane-bound organelles, Curr. Opin. Cell Biol. 26 (2014) 79–86.
[28] T. Niki, J. Endo, K. Takahashi-Niki, T. Yasuda, A. Okamoto, Y. Saito, H. Ariga, S.M.M. Iguchi-Ariga, Dj-1-binding compound b enhances nrf2 activity through the pi3-kinase-akt pathway by dj-1-dependent inactivation of pten, Brain Res. 1729

(2020) 146641.
[29] Z. Su, J.G. Burchfield, P. Yang, S.J. Humphrey, G. Yang, D. Francis, S. Yasmin, S.Y. Shin, D.M. Norris, A.L. Kearney, M.A. Astore, J. Scavuzzo, K.H. Fisher-Wellman, Q.P. Wang, B.L. Parker, G.G. Neely, F. Vafaee, J. Chiu, R. Yeo, P.J. Hogg, D.J. Fazakerley, L.K. Nguyen, S. Kuyucak, D.E. James, Global redox proteome and phosphoproteome analysis reveals redox switch in akt, Nat. Commun. 10 (2019) 5486.
[30] Y. Zhao, W. Song, Z. Wang, Z. Wang, X. Jin, J. Xu, L. Bai, Y. Li, J. Cui, L. Cai, Resveratrol attenuates testicular apoptosis in type 1 diabetic mice: role of akt-mediated nrf2 activation and p62-dependent keap1 degradation, Redox Biol. 14 (2018) 609–617.
[31] Y. Liu, Y. Li, J. Ni, Y. Shu, H. Wang, T. Hu, Mir-124 attenuates doxorubicin-induced cardiac injury via inhibiting p66shc-mediated oxidative stress, Biochem. Biophys. Res. Commun. 521 (2020) 420–426.
[32] K. Shu, Y. Zhang, Protodioscin protects pc12 cells against oxygen and glucose deprivation-induced injury through mir-124/akt/nrf2 pathway, Cell Stress Chaperones 24 (2019) 1091–1099.
[33] I. Rezuchova, S. Hudecova, A. Soltysova, M. Matuskova, E. Durinikova, B. Chovancova, M. Zuzcak, M. Cihova, M. Burikova, A. Penesova, L. Lencesova, J. Breza, O. Krizanova, Type 3 inositol 1,4,5-trisphosphate receptor has anti-apoptotic and proliferative role in cancer cells, Cell Death Dis. 10 (2019) 186.
[34] C.W. Distelhorst, M.D. Bootman, Creating a new cancer therapeutic agent by targeting the interaction between bcl-2 and ip3 receptors, Cold Spring Harb. Perspect. Biol. 11 (2019).
[35] A. Bartok, D. Weaver, T. Golenar, Z. Nichtova, M. Katona, S. Bansaghi, K.J. Alzayady, V.K. Thomas, H. Ando, K. Mikoshiba, S.K. Joseph, D.I. Yule, G. Csordas, G. Hajnoczky, Ip3 receptor isoforms differently regulate er-mitochondrial contacts and local calcium transfer, Nat. Commun. 10 (2019) 3726.
[36] S. Marchi, M. Marinello, A. Bononi, M. Bonora, C. Giorgi, A. Rimessi, P. Pinton, Selective modulation of subtype iii ip(3)r by akt regulates er ca(2)(+) release and apoptosis, Cell Death Dis. 3 (2012) e304.
[37] W. Zheng, L. Talley Watts, D.M. Holstein, J. Wewer, J.D. Lechleiter, P2y1r-initiated, ip3r-dependent stimulation of astrocyte mitochondrial metabolism reduces and partially reverses ischemic neuronal damage in mouse, J. Cerebr. Blood Flow Metabol. 33 (2013) 600–611.
[38] H. Li, Y. Xie, N. Zhang, Y. Yu, Q. Zhang, S. Ding, Disruption of ip(3)r2-mediated ca(2)(+) signaling pathway in astrocytes ameliorates neuronal death and brain damage while reducing behavioral deficits after focal ischemic stroke, Cell Calcium 58 (2015) 565–576.
[39] W. Farwell, A. Simonyi, H. Scott, J.P. Zhang, V. Carruthers, R. Madsen, J. Johnson, G.Y. Sun, Effects of ischemic tolerance on mrna levels of ip3r1, beta-actin, and neuron-specific enolase in hippocampal ca1 area of the gerbil brain, Neurochem. Res. 23 (1998) 539–542.
[40] E. Nagata, K. Tanaka, S. Suzuki, T. Dembo, Y. Fukuuchi, A. Futatsugi, K. Mikoshiba, Selective inhibition of inositol 1,4,5-triphosphate-induced ca2+ release in the ca1 region of the hippocampus in the ischemic gerbil, Neuroscience 93 (1999) 995–1001.
[41] C.S. Uhm, Y.S. Suh, J.B. Park, M.B. Sohn, I.J. Rhyu, H. Kim, Mk-801, a non-competitive nmda receptor antagonist, prevents postischemic decrease of inositol 1,4,5-trisphosphate receptor mrna expression in mongolian gerbil brain, Neurosci. Lett. 255 (1998) 111–114.
[42] J. Duan, J. Cui, Z. Yang, C. Guo, J. Cao, M. Xi, Y. Weng, Y. Yin, Y. Wang, G. Wei, B. Qiao, A. Wen, Neuroprotective effect of apelin 13 on ischemic stroke by activating ampk/gsk-3beta/nrf2 signaling, J. Neuroinflammation 16 (2019) 24.
[43] G.Y. Sun, J.P. Zhang, T.A. Lin, T.N. Lin, Y.Y. He, C.Y. Hsu, Inositol trisphosphate, polyphosphoinositide turnover, and high-energy metabolites in focal cerebral ischemia and reperfusion, Stroke 26 (1995) 1893–1900.
[44] T. Araki, H. Kato, H. Hara, K. Kogure, Postischemic binding of [3h]phorbol 12,13-dibutyrate and [3h]inositol 1,4,5-trisphosphate in the gerbil brain: an autoradiographic study, Neuroscience 46 (1992) 973–980.
[45] G.Y. Sun, C.Y. Hsu, Poly-phosphoinositide-mediated messengers in focal cerebral ischemia and reperfusion, J. Lipid Mediat. Cell Signal 14 (1996) 137–145.
[46] A. Nishida, K. Emoto, M. Shimizu, T. Uozumi, S. Yamawaki, Brain ischemia decreases phosphatidylcholine-phospholipase d but not phosphatidylinositol-phospholipase c in rats, Stroke 25 (1994) 1247–1251.
[47] X. Gao, J. Zhang, Akt signaling dynamics in plasma membrane microdomains visualized by fret-based reporters, Commun. Integr. Biol. 2 (2009) 32–34.
[48] B.D. Goulden, J. Pacheco, A. Dull, J.P. Zewe, A. Deiters, G.R.V. Hammond, A high-avidity biosensor reveals plasma membrane pi(3,4)p2 is predominantly a class i pi3k signaling product, J. Cell Biol. 218 (2019) 1066–1079.
[49] K. Homma, S. Terui, M. Minemura, H. Qadota, Y. Anraku, Y. Kanaho, Y. Ohya, Phosphatidylinositol-4-phosphate 5-kinase localized on the plasma membrane is essential for yeast cell morphogenesis, J. Biol. Chem. 273 (1998) 15779–15786.
[50] X. Wu, R.J. Chi, J.M. Baskin, L. Lucast, C.G. Burd, P. De Camilli, K.M. Reinisch, Structural insights into assembly and regulation of the plasma membrane phosphatidylinositol 4-kinase complex, Dev. Cell 28 (2014) 19–29.
[51] J.P. Zewe, R.C. Wills, S. Sangappa, B.D. Goulden, G.R. Hammond, Sac1 degrades its lipid substrate ptdins4p in the endoplasmic reticulum to maintain a steep chemical gradient with donor membranes, eLife 7 (2018).
[52] T.R. Doeppner, M. Doehring, E. Bretschneider, A. Zechariah, B. Kaltwasser, B. Muller, J.C. Koch, M. Bahr, D.M. Hermann, U. Michel, Microrna-124 protects against focal cerebral ischemia via mechanisms involving usp14-dependent rest degradation, Acta Neuropathol. 126 (2013) 251–265.
[53] S. Hamzei Taj, W. Kho, A. Riou, D. Wiedermann, M. Hoehn, Mirna-124 induces neuroprotection and functional improvement after focal cerebral ischemia, Biomaterials 91 (2016) 151–165.
[54] T.R. Doeppner, B. Kaltwasser, E.H. Sanchez-Mendoza, A.B. Caglayan, M. Bahr, D.M. Hermann, Lithium-induced neuroprotection in stroke involves increased mir-124 expression, reduced re1-silencing transcription factor abundance and decreased protein deubiquitination by gsk3beta inhibition-independent pathways, J. Cerebr. Blood Flow Metabol. 37 (2017) 914–926.
[55] J. Yang, X. Zhang, X. Chen, L. Wang, G. Yang, Exosome mediated delivery of mir-124 promotes neurogenesis after ischemia, Mol. Ther. Nucleic Acids 7 (2017) 278–287.